

Lung Nodule Retrieval by Integrating Local Binary Pattern with Template Matching

G. Deep*¹, L. Kaur² and S. Gupta³

¹Department of CSE, IET Bhaddal, Ropar, Punjab, Punjab Technical University, India

²Department of CE, Punjabi University, Patiala, Punjab, India

³Department of CSE, UIET, PU, Chandigarh, India

Address for

Correspondence

Department of CSE,
IET Bhaddal, Ropar,
Punjab, India.
(Punjab Technical
University, Jalandhar)

E-mail:

gaganpec@yahoo.com

ABSTRACT

This paper focuses on the use of local binary pattern (LBP) in template matching for nodule retrieval from CT lung images. Existing local binary pattern operators uses the features of LBP to train the classifiers for the classification of lung nodules, here LBP method is used for the extraction of features from lung nodule images. In this work, LBP method is applied on both the lung images as well as on nodule templates to extract LBP features. The resulting features are compared to extract the cancerous nodules. Experiments are performed on the lung data sets collected from LIDC database. The results show that use of LBP features in template matching yields better accuracy rate as compared to the literature.

Keywords: lung nodules, rotation invariant LBP variance, segmentation, nodule templates, template matching.

INTRODUCTION

In the past two decades numerous screening studies have been conducted worldwide to study early indications of lung cancer. Indeed, survival of lung cancer is strongly dependent on accurate and early diagnosis¹. The early clinical diagnosis generally begins with retrieval of lung nodules from Computed Tomography (CT) images. For identifying the lung nodules, CT scan of the thorax is widely applied in diagnosis. Compared to other modalities, CT excels in the imaging of the lungs². Many researchers have worked on lung nodule retrieval from CT images in the past several years. There are two main approaches for

lung nodules retrieval: classifier-based method and template matching ones. Classification methods utilize image texture descriptors³. Texture is very important component as in³³. The local binary patterns⁴ (LBP), is most widely used texture descriptor because of its low computational complexity and capacity to code minute specifications. In the field of medicine, for instance⁵ successfully used LBP descriptor for mammogram images, and ⁶introduced a powerful search and retrieval method that used LBP with Support Vector Machines (SVMs) to find relevant slices in brain magnetic resonance volumes. Keramidas *et*

*al.*⁷ have given texture representation on thyroid ultrasound images. In 2008, Nanni *et al.*^{8,9} used LBP to automate the cell phenotype image classification. In the area of face classification,¹⁰ and¹¹ have extensively worked on LBP. Some important papers^{12,13} have also successfully experimented LBP in other useful applications. More on LBP can be explored at http://www.ee.oulu.fi/mvg/page/lbp_bibliography#biomedical. Although classifiers designed using LBP yields high accuracy rate, but also produces a high false-positive (FP) rate and is computationally expensive¹⁴.

Other method for lung nodule retrieval is template matching. There are some of approaches derived from template matching-based method, including those based on the deformation of the object, and methods based on anatomy Models^{15,16}. A novel genetic algorithm (GA) based template matching technique (GATM) to detect nodules was proposed in¹⁷. In¹⁸, an algorithm for nodule detection was designed, that used deformable 3D and 2D templates describing typical geometry and gray level distribution within the nodules of the same type. The detection combines normalized cross-correlation (NCC) template matching by genetic optimization and Bayesian post-classification. Many methods were designed based on gray level changes, with good sensitivity rate¹⁹, 92.3% and with reduced FP²⁰ to 9.2%. In²¹, templates based on the spherical enhancement, using 3D geometric feature calculation and the shape based on GATM template matching algorithm are designed. 3D reconstruction design on the basis of the template matching method²² is made with the accuracy of 84.84%. Different machine learning techniques, including template matching, support vector machines, linear discriminant analysis and the linear programming technique, are available to match lung nodule characteristics^{23,34}. For templates without strong features, a template-based approach using Sum of Absolute

Differences (SAD) measure is effective³².

In this paper, LBPV, a combination of LBP method (that recognizes certain patterns, termed “uniform patterns”) with the rotational invariant variance measure (that characterizes the contrast of the local image texture as basis) is used for template matching to retrieve different types of lung nodules. It is developed as an efficient approach for lung nodule retrieval due to high robustness of the local binary pattern method and its characteristics like rotation and scale invariance. This approach is computationally less expensive and yields reduction in the false positive rate.

The remainder of this paper is organized as follows. Section 2 describes the block representation of nodule retrieval system and also explains the use of rotation invariant LBP in template matching. Experimental results and discussion are presented in section 3. Finally the concluding remarks and directions for future research are given in section 4.

MATERIAL AND METHOD

Overall scheme of LBP in template matching

The steps of the proposed scheme of local binary pattern in template matching for lung nodule retrieval in CT images are shown in figure 1. In the first step, CT database of lung images is downloaded from Lung Image Database Consortium (LIDC) of National Cancer institute (NCI)²⁴ and then, lung images are converted in jpeg format using lossless image conversion to retain the quality and information present in image. Secondly, segmentation of CT images is performed to get lung parenchyma. Next, in the third step, rotational invariant local binary pattern method with variance measures is applied on both the segmented lung parenchymas and designed nodule templates of various sizes^{25,26} for lung nodule segmentation. In the further step, matching is done between feature vectors from the previous step using the sum

of absolute differences (SAD) method³². The final matching results are labeled as cancerous nodules on the original images.

Lung parenchyma fields segmentation

Some radiologists of Postgraduate Institute of Medical Education & Research (PGIMER), Chandigarh, INDIA suggested to remove the mediastinum part (central Part) from lung images as it is difficult to determine the malignancy at that place even for medical professionals. To view the same, the lung parenchyma fields are separated. The process of lung parenchyma field's segmentation is according to the following steps used in²⁷ as shown in figure 2.

1. Optimal Thresholding: The image is thresholded to extract low-density tissue region (e.g. Lung parenchymas) from fat area.
2. Background removal: The surrounding air, identified as low-density tissue, is removed.
3. Cleaning: It is performed to fill the holes in the binary image.
4. Lung mask: To extract lungs from background, lung mask is created.
5. Lung Extraction: Output of step 4 is subtracted from the original image to provide separated lung parenchymas for further processing.

Local binary pattern formulation

After obtaining lung parenchymas from the preprocessing step, the LBPV operator is applied on lung data set and nodule templates. Ojala *et al.*⁴ first introduced the *LBP* operator for rotation invariant texture classification. The *LBP* is very efficient texture descriptor due to its discriminative power and computational simplicity. Given an image *I* of size $n \times m$ grayscale pixels and we denote with $I(g)$ gray level of the *g*th pixel of the image *I*, the *LBP* operator is calculated at each pixel by evaluating the binary differences of the values of a small

circular neighborhood (with radius *R*) around the value of a central pixel g_c . Mathematically, the *LBP* value of current pixel is given:

$$LBP_{P,R} = \sum_{p=0}^{P-1} s(g_p - g_c) 2^p,$$

$$s(x) = \begin{cases} 1, & \text{if } x \geq 0; \\ 0, & \text{otherwise;} \end{cases} \quad (1)$$

where

g_c : gray value of the center pixel

g_p : gray values of the circularly symmetric neighborhood g_p ($p = 0, \dots, P-1$).

P: Image Pixels in the circle of radius *R* ($R > 0$) that form a circularly symmetric neighbor set respectively

2^p : binomial factor for each sign $s(g_p - g_c)$

A histogram is generated to represent the texture image after finding the *LBP* code of each pixel in the image. Figure 3 shows *LBP* derivation with example using 3x3 neighborhood. In this, each *LBP* is regarded as a micro-texton⁴.

Local textons include spots, flat areas, edges, line ends and corners. Figure 4 shows the different texture primitives detected by the uniform patterns of *LBP*. In the figure 4, gray circle indicates center pixel, Black and white circles correspond to bit values of 0 and 1 in the different patterns of the operator.

Rotation invariance⁴

To remove the effect of rotation, each *LBP* code must be rotated back to a reference position, effectively making all rotated versions of a binary code the same. This transformation is defined as follows:

$$LBP_{P,R}^{ri} = \min \{ ROR(LBP_{P,R}, i) \mid i=0, \dots, P-1 \} \quad (2)$$

where the superscript '*ri*' stands for "rotation invariant", the function $ROR(x, i)$ performs '*i*' times bit-wise circular right shift on the *P* bit binary number, *x*. In terms of image pixels,

this simply corresponds to rotating the neighbor set clockwise so as to get maximum number of zeros in the beginning of the binary string⁴; ‘min’ operator will just take the minimum decimal values from different patterns.

Uniform Pattern⁴

Sometimes rotation invariant patterns cannot give good discrimination⁴. Some patterns among rotation invariant patterns are dominant, and are fundamental properties of texture. The patterns are considered uniform, if the number of transitions between 0 and 1 are less than or equal to two in the circular binary code. This operator is called $LBP_{P,R}^{riu2}$. Non uniform patterns are considered the patterns that contain the main part of the noise of the images. A region with no transitions is considered as a background or a flat region of the image. The LBP feature vector is extracted from each cell and is the histogram of dimension $P + 2$ (a single bin for non-uniform patterns). $LBP_{P,R}^{riu2}$ operator is formally defined as⁴

$$LBP_{P,R}^{riu2} = \begin{cases} \sum_{p=0}^{P-1} s(g_p - g_c), & \text{if } U(LBP_{P,R}) \leq 2 \\ P+1, & \text{otherwise,} \end{cases} \quad (3)$$

where

$$U(LBP_{P,R}) = |s(g_{P-1} - g_c) - s(g_0 - g_c)| + \sum_{p=0}^{P-1} |s(g_p - g_c) - s(g_{p-1} - g_c)| \quad (4)$$

where superscript 'riu2' denotes the rotation invariant “uniform” patterns that have U values at most of 2. Therefore, mapping from $LBP_{P,R}$ to $LBP_{P,R}^{riu2}$ results in only $p+1$ distinct groups of patterns, leading to a much shorter histogram representation for the whole image. To achieve rotation invariance, a Look-Up Table (LUT) is used. The LUT store all the possible uniform patterns along with their unique $LBP_{8,R}^{riu2}$ code.

In conventional LBP the central pixel is discarded (despite the implicit use of the intensity of the central pixel as the threshold to achieve local gray-scale invariance), and only the joint distribution of the neighborhood around each pixel is considered. The LBP oversimplifies local structure and loses textural information⁴. Therefore, Ojala *et al.*⁴ made a correction by including the local contrast of each pattern and proposing a complementary local descriptor called $VAR_{P,R}$. Using the joint histogram of $LBP_{P,R}^{riu2}$ and $VAR_{P,R}$ denoted as $LBP_{P,R}^{riu2}/VAR_{P,R}$ (Aka $LBPV$), a powerful tool for rotation invariant texture classification is demonstrated in⁴.

$$VAR_{P,R} = \frac{1}{P} \sum_{p=0}^{P-1} (g_p - \mu)^2, \quad \text{where } \mu = \frac{1}{P} \sum_{p=0}^{P-1} g_p \quad (5)$$

Template matching

To identify the lung nodule from local binary pattern variance image, the different size of rotational invariant LBP templates nodules are matched using template matching. A basic method of template matching uses a template, tailored to a specific feature of the search image, which one want to detect. Then, simply moves the center (or the origin) of the template T over each (x, y) point in the search image. Here, SAD (Sum of absolute differences) measure³² is used for matching the intensities of the pixels. Let $I_s(x_s, y_s)$ represents intensity of a pixel at coordinates (x_s, y_s) in the search image and $I_t(x_t, y_t)$ denotes the intensity of a pixel at coordinates (x_t, y_t) in the template. Thus the absolute difference in the pixel intensities is defined as

$$Diff(x_s, y_s, x_t, y_t) = |I_s(x_s, y_s) - I_t(x_t, y_t)|.$$

$$SAD(x, y) = \sum_{i=0}^{T_{rows}} \sum_{j=0}^{T_{cols}} Diff(x+i, y+j, i, j) \quad (6)$$

where, T_{rows} and T_{cols} denote the rows and the columns of the template image respectively.

The mathematical representation for the looping through the pixels in the search image as we translate the center of the template at every pixel and take the SAD measure is the following:

$$\sum_{x=0}^{S_{rows}} \sum_{y=0}^{S_{cols}} SAD(x, y) \quad (7)$$

where S_{rows} and S_{cols} represent the rows and the columns of the search image.

The lowest value of SAD score gives the estimate for the best position of template within the search image.

The local binary pattern and variance measures information with the use of descriptor $LBP_{P,R}^{riu2}/VAR_{P,R}$ at different rotation angles ($\beta \in \{0^0, 45^0, 60^0, 90^0\}$) is stored in the form of image histograms for both lung images and nodule templates and in the next step, feature information uses in the template matching instead of classifiers.

EXPERIMENTAL RESULTS AND DISCUSSION

The experiments are conducted on the images collected from LIDC public lung image database²⁴. The database is separated into 84 cases, each containing around 100-400 Digital Imaging and Communication (DICOM) images and an XML data file containing the physicians annotations. Database contains 143 nodules having size range of 3 to 30mm (to be manually segmented by radiologists). The size of nodule template is taken using the characteristics of the medical lung nodule templates²⁶. The lung nodule templates are designed in the range of 4-20 mm in diameter. This size is chosen by calculating the area of standard affected nodules in the area of medical field. Further, the lung nodules are processed using various morphological operations to give the final shape. The lung

nodule templates types with different sizes are shown in figure 5.

In this paper, the goal is to enhance the performance of template matching with the rotation invariant uniform patterns by extracting a set of features from the extracted lung parenchymal field segmented image. The histogram from the uniform pattern image represents the number of uniform patterns present in the image corresponding to predefined 256 mapping uniform patterns possible when a neighborhood of size 3×3 is used. The $LBP_{1,8}^{riu2}$ image and its histogram are shown in figure 6 (a) and 6 (b) respectively. The final combined operator $LBP_{P,R}^{riu2}/VAR_{P,R}$ separates the texture with clear boundaries resulting in very efficient segmentation of image (figure 6 (c)). In practice, same (P, R) values are used for $LBP_{P,R}^{riu2}$ and $VAR_{P,R}$. Each texture is captured in four rotation angles ($\beta \in \{0^0, 45^0, 60^0, 90^0\}$).

The template is rotated at different angles ($\beta \in \{0^0, 45^0, 60^0, 90^0\}$) and LBP operator is applied at each orientation of template. The feature vector of nodule templates contain the rotation invariant LBP variance measure at different angles of ($\beta \in \{0^0, 45^0, 60^0, 90^0\}$) and correspondingly histograms of patterns for rotation invariant features are shown in figures 7(a) (b) (c) (d).

The features obtained from the uniform patterns in the histograms of rotation invariant lung images and rotation invariant nodule templates match with each other at different orientations using SAD measure. The extracted lung nodules are marked with red color (as shown in figure 8).

For the quantitative evaluation of lung nodule retrieval method, the commonly used metrics like *Accuracy*, *Sensitivity*, *False Negatives (FN)* and *False Positive (FP)* are computed. High level of accuracy rate, Sensitivity rate and low FP rate represent a good retrieval method. The metrics are defined as in^{28,29}.

$$\text{Accuracy} = ((TP + TN))/((TP + FP + FN + TN)) \quad (8)$$

$$\text{sensitivity} = TP/(TP + FN) = \text{probability of positive test given that the patient is ill} \quad (9)$$

$$\text{specificity} = TN/(TN + FP) = \text{probability of negative test given that the patient is well} \quad (10)$$

$$\text{False Positive rate} = 1 - \text{specificity} = FP/(FP + TN) \quad (11)$$

$$\text{False Negative rate} = 1 - \text{sensitivity} = FN/(TP + FN) \quad (12)$$

where TN stands for true negative and TP stands for true positive,

Table 1 represents the average accuracy obtained by the LBP variance method on LIDC datasets for identification of parenchymal nodules of sizes 10mm, 15mm, 20mm and Juxtapleural nodules of size 18mm. The results are taken on a series of 50 patient's images. The values in the table show that LBP method yield average accuracy higher than 94% that is more than 94% cases will be correctly diagnosed for ailment. To demonstrate the effectiveness of the local binary pattern method on cancerous nodule retrieval, metrics like sensitivity and specificity are computed on 40 sets of DICOM CT lung cancer images (Table 2). The results are presented at different neighborhood sizes (by varying radius ($R=1, 2$) and number of pixels ($P = 8, 16$)) are shown in Table 2. The numerical values of the metrics indicate that LBP rotation invariant method produces average sensitivity higher than 98% and specificity 93% (see Table 2). Whereas, already developed computer aided diagnosis system for pulmonary nodule detection in CT imagery had given the specificity of 80.4% and

sensitivity of 82.66% on LIDC database³⁰.

The experimental results are also compared with the specificity and sensitivity of evaluation of linear binary pattern feature descriptors for detection and classification of lung nodules in CT scans of the chest³¹.

Further, the curve tradeoff between sensitivity and specificity for different nodule sizes of 10, 15, 20 mm of parenchymal and 18 mm of Juxtapleural are shown in figure 9. The figures reveal that at specificity of 93%, sensitivity of system is close to 99 percent which suggest the system is highly capable of lung nodule detection. Thus, it can be concluded that rotation invariant LBP based template matching method provides a powerful mechanism to diagnosis for doctors.

Here, in this paper, the results show that use of LBP features in template matching yields better accuracy rate as compared to the literature. So, it is developed as an efficient approach for lung nodule retrieval due to high robustness of the local binary pattern method and its characteristics like rotation and scale invariance. From the experiments, this approach is computationally less expensive and yields reduction in the false positive rate.

CONCLUSIONS AND FUTURE WORK

In this paper, the applicability of LBP variance operator on lung nodule retrieval is analyzed. The images are collected from publicly available LIDC database. The combined gray-scale invariant LBP and rotational invariant variance measure $LBP_{P,R}^{riu2}/VAR_{P,R}$ is used to extract feature vectors from lung image dataset and the nodule templates, and then the template matching method is implemented to retrieve the lung nodules. It is experimentally shown that LBP based method has excellent performance in the template matching as it yields high accuracy, high sensitivity and specificity. In the future work, some criteria of optimality can be used to process number of images in the datasets. The semantic

information can be extracted from DICOM header of DICOM CT images which can be used to perform the initial search to retrieve the images. This pre-filtering of the images can reduce the number of images to be searched and speed up the retrieval process.

The accuracy of system is dependent on nodule template. The accuracy of process can greatly be increased if medical fraternity will provide templates of nodules that come under malignant category.

ACKNOWLEDGMENTS

The authors thank Dr. N. Khandelwal, Professor & Head, Department of Radio-diagnosis, PGIMER, Chandigarh, India for giving valuable suggestions to retrieve the lung nodules from CT lung images. We also wish to express our appreciation to the Lung Image Database Consortium and other institutions who contributed to the creation of the LIDC collection used here as an independent testing data set.

REFERENCES

1. United States National Institute of Health. Internet: www.nih.gov.
2. M. Prokop I. Sluimer, A. Schilham, B. van Ginneken. "Computer analysis of computed tomography scans of the lung: A survey." *IEEE Transactions on Medical Imaging*, 25(4), pp.385-405, 2006
3. Zhang, B., Gao, Y., Zhao, S., & Liu, J. "Local derivative pattern versus local binary pattern: Face recognition with high-order local pattern descriptor." *IEEE Transactions on Image Processing*, 19(2), pp.533–544, 2010.
4. Ojala, T., Pietikainen, M., & Maenpaa, T. "Multiresolution gray-scale and rotation invariant texture classification with local binary patterns." *IEEE Transactions on Pattern Analysis and Machine Intelligence*, 24(7), pp.971–987, 2002.
5. Oliver, A., Lladó, X., Freixenet, J., & Martí, J. "False positive reduction in mammographic mass detection using local binary patterns." In *Proceedings of the medical image computing and computer-assisted intervention (MICCAI 2007)*. Lecture Notes in Computer Science 4791 (Vol. I), 2007, pp. 286–293.
6. Unay, D., & Ekin, A. "Intensity versus texture for medical image search and retrieval." In *Proceedings of the fifth IEEE international symposium on biomedical imaging: From nano to macro*, 2008, pp. 241–244.
7. Keramidas, E.G., Iakovidis, D.K., Maroulis, D., & Dimitropoulos, N. "Thyroid texture representation via noise resistant image features." In *Proceedings of the 21st IEEE international symposium on computer-based medical systems*, 2008, pp. 560–565.
8. Nanni, L., & Lumini, A. "A reliable method for cell phenotype image classification." *Artificial Intelligence in Medicine*, 43(2), pp.87–97, 2008b.
9. Nanni, L., & Lumini, A. "Ensemble of neural networks for automated cell phenotype image classification." *Biomedical image analysis and machine learning technologies: Applications and techniques*, 2008c.
10. Nanni, L., & Lumini, A. "Region Boost learning for 2D + 3D based face recognition." *Pattern Recognition Letters*, 28(15), pp.2063–2070, 2007.
11. Ahonen, T., Hadid, A., & Pietikainen, M. "Face description with local binary patterns: Application to face recognition." *IEEE TPAMI*, 28(12), pp.2037–2041, 2006.
12. Nanni, L., & Lumini, A. "Local binary patterns for a hybrid fingerprint matcher." *Pattern Recognition* (11), pp.3461–3466, 2008.
13. Shang, X., & Veldhuis, R. "Local absolute binary patterns as image preprocessing for grip-pattern recognition in smart gun." In *Proceedings first IEEE international conference on biometrics: Theory, applications, and systems*, 2007, pp.1–6.
14. Saba, L., Caddeo, G., Mallarini, G. "Computer-aided detection of pulmonary nodules in computed tomography: analysis and review of the literature." *Journal of Computer Assisted Tomography* 31(4), pp.611–619, 2007.
15. Zhang, H., Chen, Z. "Research on Classical Image Matching Algorithm and Its Improved Method." *Exploitation and Application of Software*, 27(9), 2008.

16. Hong, H., Lee, J., Yim, Y. "Automatic lung nodule matching on sequential CT images." *Computers in Biology and Medicine*, 38(5), pp.623–634, 2008.
17. Lee, Y., *et al.* "Automated detection of pulmonary nodules in helical CT images based on an improved template-matching technique." *IEEE Transactions on Medical Imaging*, 20(7), pp.595–604, 2001.
18. Farag, A.A., *et al.* "Detection and recognition of lung abnormalities using deformable templates." In: *Proceedings of the 17th International Conference on Pattern Recognition*, 2004, vol. 3, pp. 738–741.
19. Ozekes, S., Camurcu, A.Y. "Automatic lung nodule detection using template matching." In: Yakhno, T., Neuhold, E.J. (eds.), 2006, vol. 4243, pp. 247–253.
20. Osman, O., Ozekes, S., Ucan, O.N. "Lung nodule diagnosis using 3D template matching." *Computers in Biology and Medicine*, 37(8), pp.1167–1172, 2007.
21. Dehmeshki, J., *et al.* "Automated detection of lung nodules in CT images using shape-based genetic algorithm." *Computerized Medical Imaging and Graphics: The Official Journal of the Computerized Medical Imaging Society*, 31(6), pp.408–417, 2007.
22. Da Silva Sousa, J.R.F., *et al.* "Methodology for automatic detection of lung nodules in computerized tomography images." *Computer Methods and Programs in Biomedicine*, 98(1), pp.1–14, 2010.
23. Caifeng Shan, Shaogang Gong, Peter W. McOwan. "Facial expression recognition based on Local Binary Patterns: A comprehensive study." *Image and Vision Computing*, vol.27, pp.803–816, 2009.
24. Kascic, E., NBIA - National Cancer Imaging Archive NCIA (version 4.0): The NCI's repository for DICOM-based images, Internat: <https://cabig.nci.nih.gov/tools/NCIA>
25. Armato III *et al.* "The lung image database consortium (LIDC) and image database resource initiative (IDRI): A completed reference database of lung nodules on CT scans." *Medical Physics*, 38 (2), 2011.
26. Leung, A., Smithuis, R. "Solitary pulmonary nodule: benign versus malignant." *The Radiology Assistant, Department of Radiology*, 2007.
27. Heuberger, J., Geissbuhler, A., Muller, H. "Lung CT segmentation for image retrieval using the Insight Toolkit (ITK)." *Medical Imaging and Telemedicine, (MIT2005)*. Hopitaux University of Geneva, China, 2005.
28. W. Zhu, N. Zeng, N. Wang. "Sensitivity, specificity, accuracy, associated confidence interval and ROC analysis with practical SAS implementations, Health care and Life Sciences." *NESUG proceedings*. 2010, pp.1-9.
29. A. S. Nair, Aswathi B.L, "Sensitivity, specificity, accuracy and the relationship between them, licensed under creative commons attribution-share alike 2.5 india license." *Centre for Bioinformatics*, 2009.
30. T. Messay, R. C. Hardie, S. K. Rogers. "A new computationally efficient CAD system for pulmonary nodule detection in CT imagery." *Med. Image Anal*, 14(3), pp.390-406, 2010.
31. Amal Farag, Asem Ali, James Graham, Aly Farag, Salwa Elshazly and Robert Falk. "Evaluation of geometric feature descriptors for detection and classification of lung nodules in low dose CT scans of the chest." *International Symposium on Biomedical Imaging*, 2011, pp.169 – 172.
32. H. Y. Kim, S. A. Araújo. "Grayscale template-matching invariant to rotation, scale, translation, brightness and contrast." *IEEE Pacific-Rim Symposium on Image and Video Technology, Lecture Notes in Computer Science*, vol. 4872, 2007, pp. 100-113.
33. T. Rajesh, M. Karnan and R. Sivakumar, "Performance Analysis of Iris Recognition System-A Review." *American Journal of Computer Science & Information Technology*, 1(1), pp. 039-050, 2013,
34. S. Ghosh and S. K. Bandyopadhyay, "A Method for Face Recognition from Facial Expression." *American Journal of Computer Science & Information Technology*, 3(4), pp. 148-166, 2015.

Table 1. Average accuracy obtained at different sizes of nodules on LIDC database

| Patient ID (Each patient ID contains many images) | Segmentation Accuracy | Accuracy at parenchymal nodule identification | | | Accuracy at Juxtapleural nodule identification |
|---|--------------------------|--|-----------------|-----------------|--|
| | | 10 mm Nodule | 15 mm Nodule | 20 mm Nodule | 18 mm Nodule |
| 1.3.6.1.4.1.9328.50.3.0041 | 98.5891 | 94.6901 | 97.1726 | 97.1686 | 97.1809 |
| 1.3.6.1.4.1.9328.50.3.0042 | 98.5161 | 95.2380 | 97.1178 | 97.1182 | 97.1239 |
| 1.3.6.1.4.1.9328.50.3.0043 | 98.5766 | 95.2407 | 97.1683 | 97.1495 | 97.1713 |
| 1.3.6.1.4.1.9328.50.3.0044 | 98.3885 | 95.0405 | 96.9904 | 96.9842 | 96.9867 |
| 1.3.6.1.4.1.9328.50.3.0045 | 98.5766 | 95.1456 | 97.4661 | 97.4514 | 97.4814 |
| 1.3.6.1.4.1.9328.50.3.0046 | 98.3365 | 95.0169 | 96.7960 | 96.7872 | 96.7993 |
| 1.3.6.1.4.1.9328.50.3.0047 | 98.5101 | 96.3748 | 96.4549 | 96.4655 | 96.4514 |
| 1.3.6.1.4.1.9328.50.3.0048 | 98.5371 | 95.1449 | 97.2132 | 97.1950 | 97.2092 |
| 1.3.6.1.4.1.9328.50.3.0050 | 98.4600 | 96.4811 | 96.2735 | 96.2701 | 96.2817 |
| 1.3.6.1.4.1.9328.50.3.0051 | 98.6191 | 95.3056 | 97.2261 | 97.2376 | 97.2351 |
| Average Accuracy | 98.51097 | 95.3678 | 96.9879 | 96.9827 | 96.9921 |

Table 2. Average performance obtained with different radius and neighborhood sizes on DICOM CT lung cancer images

| Nodule Types of various sizes | Performance of LBP descriptors in Template Matching in terms of metrics: | | | |
|----------------------------------|--|-------------|--------------------------|--------------------------|
| | Specificity | Sensitivity | False Positive (FP) rate | False Negative (FN) rate |
| All Nodule types | | | | |
| PARENCHYMAL NODULE OF SIZE 10mm | 93.7857 | 98.3627 | 6.2143% | 1.6373% |
| PARENCHYMAL NODULE OF SIZE 15mm | 93.7004 | 99.7589 | 6.2996% | 0.2411% |
| PARENCHYMAL NODULE OF SIZE 20mm | 93.6992 | 99.7578 | 6.3008% | 0.2422% |
| JUXTAPLEURAL NODULE OF SIZE 18mm | 93.7139 | 99.7571 | 6.2861% | 0.2429% |

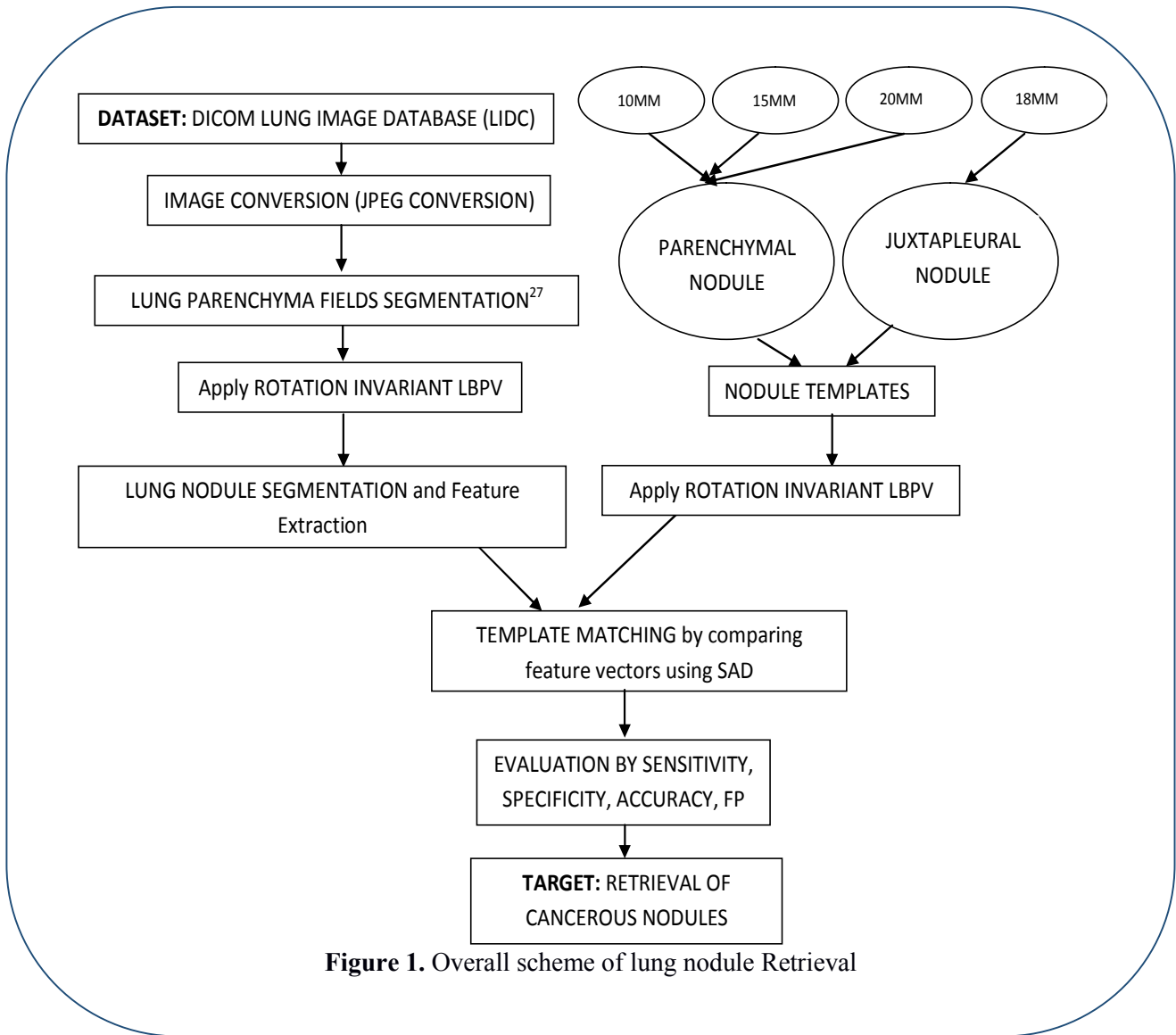
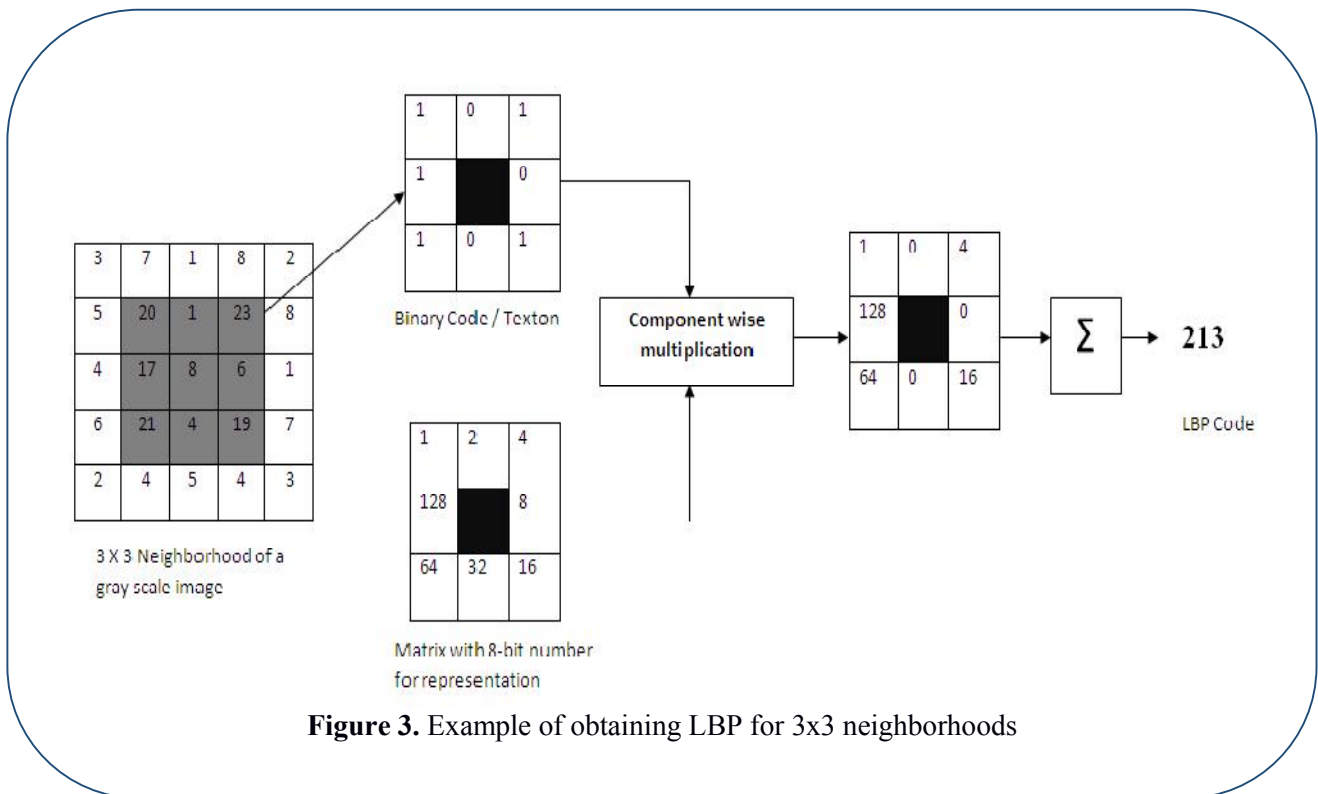
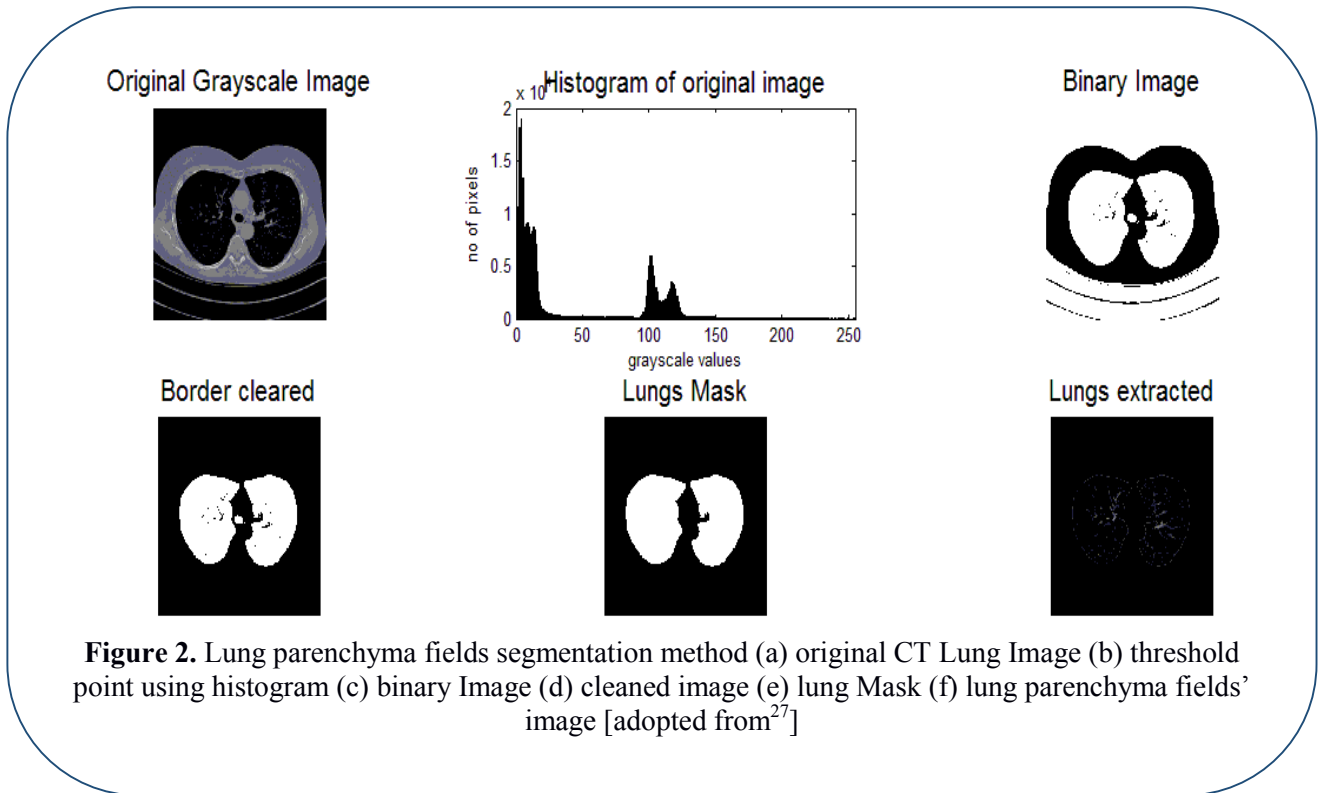


Figure 1. Overall scheme of lung nodule Retrieval



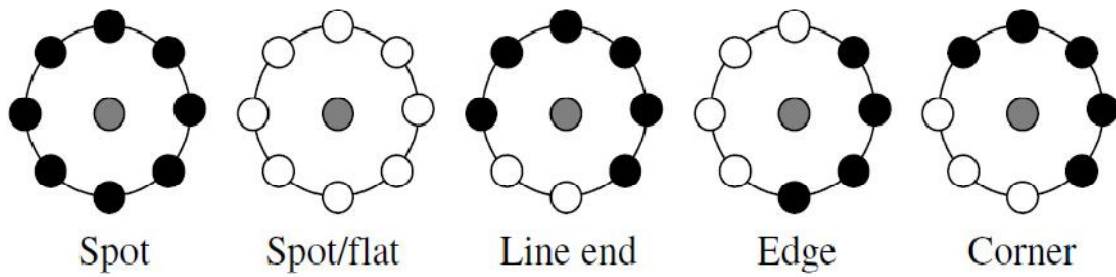


Figure 4. Different texture primitives detected by the uniform patterns of LBP⁴

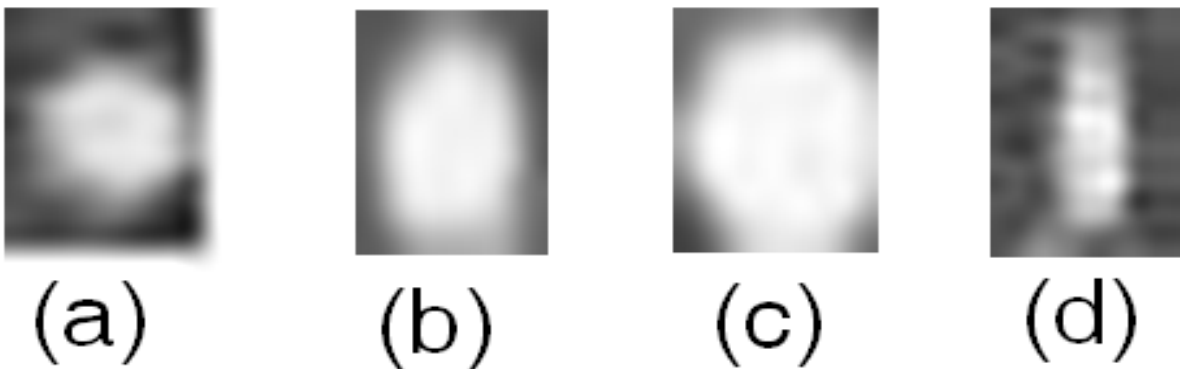


Figure 5. Nodule Templates of different types: (a), (b), (c) shows the Parenchymal nodule templates of diameter 10, 15, 20mm respectively, (d) Juxtaleural nodule template of diameter 18 mm

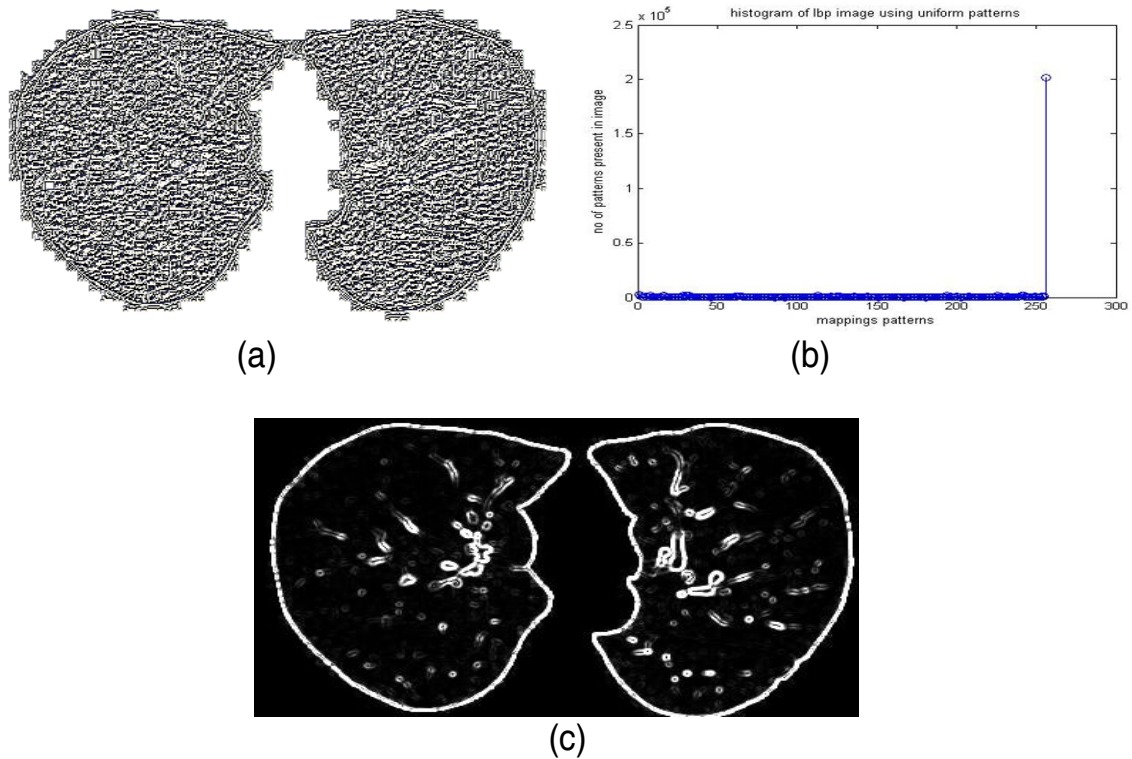


Figure 6. Rotation invariant LBP operations on lung images (a) rotation invariant $LBP_{1,8}^{riu2}$ (b) histogram showing number of uniform pattern in the image (c) segmented lung image using $LBP_{P,R}^{riu2} / VAR_{P,R}$ operator with different values of P, R and on the rotation angles of ($\beta \in \{0^\circ, 45^\circ, 60^\circ, 90^\circ\}$)

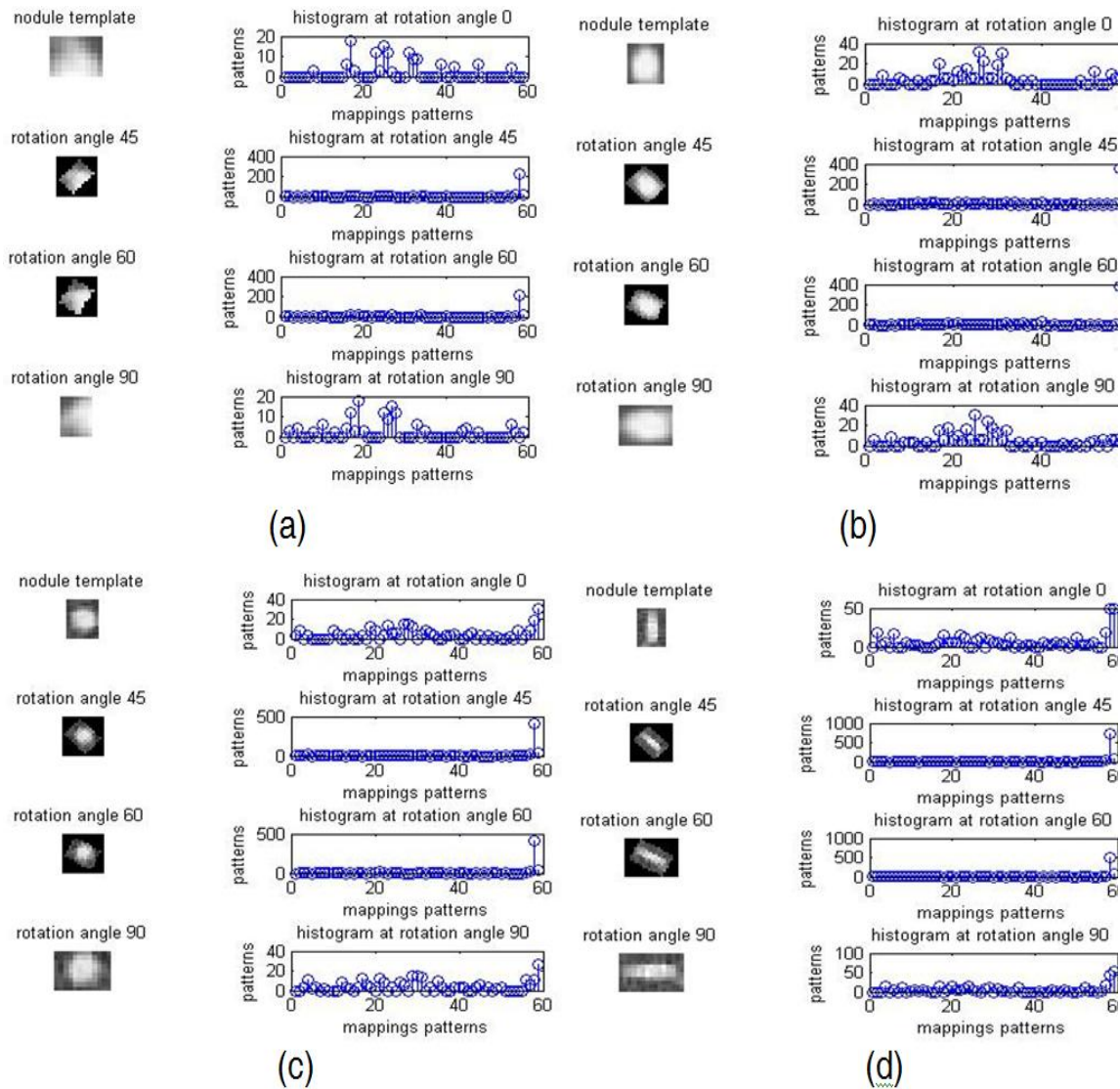
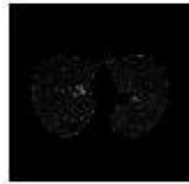


Figure 7. Rotation invariant lung templates (a) (b) (c) Rotation invariant templates of Parenchymal nodule of different sizes of 10mm, 15mm, 20mm respectively, (d) Rotation invariant template of Juxtapleural nodule of size 18mm at different rotation angles ($\beta \in \{0^\circ, 45^\circ, 60^\circ, 90^\circ\}$)

original lungs image nodule with radius 10 mm nodule with radius 15 mm



nodule with radius 20 mm

juxtapaxteral nodule

cancerous nodules



Figure 8. Output showing marking of corresponding nodules a) original image b) image marked with parenchymal nodules of size 10 mm c) parenchymal nodule with radius 15 mm d) parenchymal nodule with 20 mm radius e) Juxtapleural nodule with radius 18 mm f) cancerous nodules

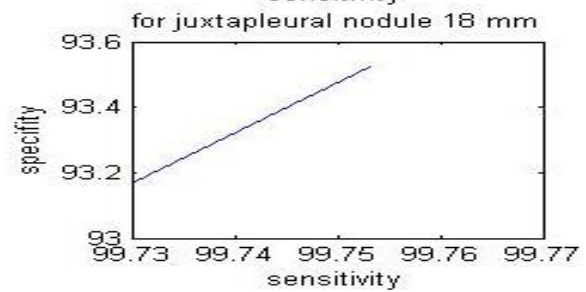
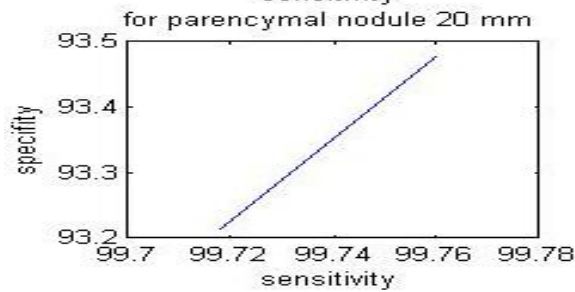
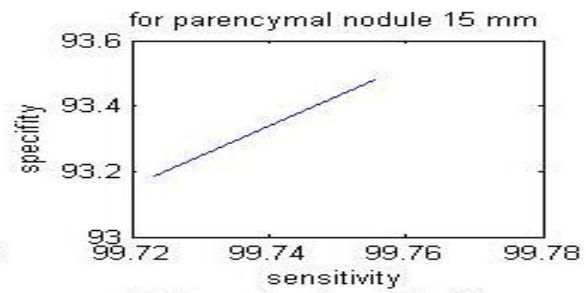
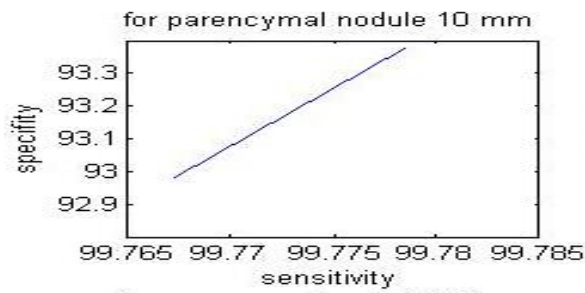


Figure 9. Curve tradeoff between sensitivity and specificity lung nodules of different sizes